Published in final edited form as:
Biochemistry. 2010 June 8; 49(22): 4662–4671. doi:10.1021/bi100320y.

Evidence that Highly Conserved Residues of Transmembrane Segment 6 of *Escherichia coli* MntH Are Important for Transport Activity

Heather A.H. Haemig[#], **Patrick J. Moen**[#], and **Robert J. Brooker**[*,#]

[#]Dept. of Genetics, Cell Biology, and Development, University of Minnesota, 321 Church St., Minneapolis, MN 55455

Abstract

Nramp (natural resistance-associated macrophage protein) family members have been characterized in mammals, yeast, and bacteria as divalent metal ion/H^+ symporters. In previous work, a bioinformatic approach was used for the identification of residues that are conserved within the Nramp family [ref.1. Haemig, H.A. and R.J. Brooker, (2004) *J Membr. Biol*, *201*(2): 97-107]. Based on site-directed mutagenesis of highly conserved negatively charged residues, a model was proposed for the metal binding site of the *E.coli* homolog, MntH. In this study, we have focused on the highly conserved residues, including two histidines, of transmembrane segment 6 (TMS-6). Multiple mutants were made at the eight conserved sites (i.e., Gly-205, Ala-206, Met-209, Pro-210, His-211, Leu-215, His-216, and Ser-217) in TMS-6 of *E. coli* MntH. Double mutants involving His-211 and His-216 were also made. The results indicate the side chain volume of these residues is critically important for function. In most cases, only substitutions that are closest in side chain volume still permit transport. In addition, the K_m for metal binding is largely unaffected by mutations in TMS-6, whereas V_{max} values were decreased in all mutants characterized kinetically. Thus, these residues do not appear to play a role in metal binding. Instead, they may comprise an important face on TMS-6 that is critical for protein conformational changes during transport. Also, in contrast to other studies, our data do not strongly indicate that the conserved histidine residues play a role in pH regulation of metal transport.

The first member of the Nramp family was identified in the early 1990s as a gene conferring host resistance to a number of pathogenic microorganisms (2). Since then, members of this family of divalent metal ion transporters have been shown to have many important functions in metal ion homeostasis, including dietary iron uptake (3), recycling of red blood cells (4), immune response to pathogenic bacteria (5), and virulence of pathogenic bacteria (6,7). Nramp family members transport divalent metal cations such as Fe^{2+} and Mn^{2+} into the cell, coupled with the movement hydrogen ions (3). Transporters belonging to the Nramp family have been identified in organisms ranging from bacteria to humans with a preference for transporting iron among eukaryotes and manganese in prokaryotic species (3,7-11).

In bacteria, the physiological role of an Mn^{2+} transporter was first proposed by Silver et al. in the 1970s (12). In *E.coli*, a gene encoding such a manganese transporter, designated *mntH*, was first characterized by two independent groups in 2000 (9,10). The *mntH* gene was found to be homologous to mammalian Nramp genes. However, the gene was named *mntH*, because the encoded protein, MntH, was found to transport manganese as its preferred substrate (9,10). Topology analysis of this protein suggests that there are 11 transmembrane segments (1,13).

[*] To whom correspondence should be addressed. Telephone: (612)624-3053. brook005@umn.edu. Fax: (612)626-6140.

Naturally occurring Nramp mutations in mice and rats (G185R) are known to inhibit function and thereby lead to defects in the dietary absorption of iron and the ability to resist infection by various bacterial pathogens (14-16). Because of its expression in macrophages, many researchers have searched for an association between Nramp1 and autoimmune or infectious diseases. Though more work is necessary, a 5′$(GT)_n$ promoter polymorphism has been found in diseases such as rheumatoid arthritis, multiple sclerosis, and meningococcal meningitis [reviewed in (17)]. In addition, evidence points to iron's key role in the onset, progression, and outcome of bacterial infections [reviewed in (18) and (19)] and competition between Nramp homologs may play an important role in pathogenesis (5).

A few mutagenesis studies of Nramp homologs have examined the roles of several highly conserved negatively charged residues in the family (1,20-23). Of particular interest to our laboratory is the DPGN motif, which is nearly 100% conserved across the family and is found in TMS-1. Of ten mutations to this region in the *E.coli* MntH homolog, only one (P35G) still maintained Mn^{2+} transport levels above background suggesting a functionally important role for this motif (1). In addition, several highly conserved acidic residues are found within transmembrane segments 1 and 3. Even conservative substitutions (i.e., Glu → Asp) to these charged residues (Glu-102, Asp-109, and Glu-112) resulted in Mn^{2+} transport at levels less than 10% of wild-type MntH or no transport activity for Mn^{2+}. From this work, we proposed a model for the metal binding site (1). According to this model, the metal binding site includes three negatively charged residues (Asp-34, Asp-109, and Glu-112) and four other nearby residues (Pro-35, Gly-36, Asn-37, and Gly-115), all of which are 100% conserved in the Nramp family.

During our sequence comparisons of Nramp family members, we also found several highly conserved residues in TMS-6, including two histidine residues. Histidine pairs have often been cited in the literature as metal binding sites in soluble (24) and membrane proteins (25,26). In recent mutagenesis studies of the conserved histidine residues of TMS-6, the histidine residues (His-211 and His-216 of *E. coli* MntH and the analogous residues in mouse Nramp2) were proposed to play a role in pH regulation of metal transport (20,21). However, neither of these studies examined the additional six highly conserved residues in this helix. In the current study, we have made multiple substitutions at these residues in *E.coli* MntH TMS-6: Gly-205, Ala-206, Met-209, Pro-210, Leu-215, and Ser-217. In addition, we have made four substitutions to each histidine (His-211 and His-216) and created four double mutant proteins for analysis. The site-directed mutants were then analyzed with regard to their effects on expression and transport. Mutations affecting the two conserved histidine residues were also examined with regard to a possible role in pH regulation of metal transport.

Materials and Methods

Reagents

$MnCl_2$ and MES (2-N-morpholino ethane sulfonic acid) and TES [N-Tris [hydroxymethyl] methyl-2-aminoethanesulfonic acid) were purchased from Sigma (St. Louis, MO). [^{54}Mn] was purchased from Perkin Elmer (Boston, MA). Restriction enzymes and DNA ligase were purchased from New England Biolabs (Beverly, MA). The QuikChange kit was purchased from Stratagene (La Jolla, CA). All remaining reagents were of analytical grade.

Bacterial strains and methods

The relevant genotypes of the bacterial strains and mutant plasmids are described in Table 1. Plasmid DNA was purified using the Eppendorf Plasmid Mini DNA Kit (Westbury, NY). Restriction digests and ligations were performed according to the manufacturers'

recommendations. Cell cultures were grown in YT media (27) supplemented with chloramphenicol (30 μg/mL).

Site-directed mutagenesis

Mutants were made using the strategies outlined in the QuikChange mutagenesis kit. The entire *mntH* coding region was sequenced to confirm each mutation. The mutations are listed in Table 1.

Mn^{2+} transport assays

Cells were grown at 37°C with shaking to mid-log phase in YT media supplemented with 15 μg/mL chloramphenicol and 0.25 mM isopropyl 1-thio-β-D-galactopyranoside. The cells were pelleted by centrifugation at 5000g for 5 min, and the resulting pellet was washed in 50 mM MES buffer, pH 6.0 and then resuspended in the same buffer at a concentration of approximately 0.5 mg of protein/mL. The cells were then diluted 100-fold in the same buffer and equilibrated at 37°C for 5-10 min before [^{54}Mn]-$MnCl_2$ (5 μCi/mL) was added. Aliquots of 200 μL were removed at appropriate time points, and the cells were captured on 0.45 μm Metricel membranes (Gelman Sciences, Inc., Ann Arbor, MI). The cells were then washed with 5-10 mL of ice-cold 50 mM MES buffer by rapid filtration. The filter with the cells was then placed in liquid scintillation fluid and counted using a Beckman LS1801 liquid scintillation counter. Channels 401-945 were used to detect photons derived from γ-radiation of $^{54}Mn^{2+}$. As a negative control, the strain MM2115/pSU2718, which lacks a functional *mntH* gene, was also subjected to Mn^{2+} transport assays (10,28). The background values from the MM2115/pSU2718 strain were subtracted from the values obtained from the strains carrying the wild-type or mutant *6HmntH* genes. For the experiments of Figures 4 and 5, a 50 mM MES buffer was also used and the pH was adjusted to 5.0, 5.5, 6.0, or 6.5.

Membrane isolation and Western blot analysis

Ten milliliters of mid-log cells grown as for transport assays were harvested by centrifugation (5000g, 10 min). The pellet was resuspended in a cell lysis buffer (50 mM TES, pH 8.0, 100 mM NaCl, 5 mM β-mercaptoethanol, 0.1 mg/mL TPCK, 0.7 μg/mL Pepstatin, and 25 μg/mL PMSF) and quickly frozen in liquid nitrogen and thawed three times. The cell suspension was then sonicated three times for 20 s each. The membrane fraction was harvested by ultracentrifugation (45000 rpm, 45 min) and the pellet was resuspended in 200 μL of extraction buffer (50 mM TES, pH 8.0, 100 mM NaCl, 250 mM imidazole, 20% glycerol, 5 mM β-mercaptoethanol, and 0.05% lauryl maltoside). Protein concentrations were determined using a modified Bradford Assay (Bio-Rad). 50 μg samples of protein were subjected to SDS-polyacrylamide gel electrophoresis, and Western blot analysis was performed according to Sambrook et al (29). The primary polyclonal antibody recognizes the RGS-6H tag (Qiagen). The secondary antibody, goat anti-mouse conjugated to alkaline phosphatase, was purchased from Sigma. The Western blot was then scanned using a Molecular Dynamics laser densitometer and analyzed by comparison to wild-type values for the same preparation and Western blot. As shown in Table 1, the values for each mutant are reported as a percentage of wild-type 6HMntH averaged from three separate preparations.

Kinetic calculations

For all mutant strains tested, apparent K_m and V_{max} values for $^{54}Mn^{2+}$ transport were determined by observing initial linear rates of transport at five external manganese concentrations (0.1, 0.2, 0.3, 0.5, and 1.0 μM final concentration of Mn^{2+}). A minimum of six transport measurements at each of the five concentrations was made for all of the mutant strains. For the wild-type strains (pMntH and p6HMntH), the data were linear to 60 seconds. For wild-type and mutant strains with high activity, 30 second and 60 second data points were taken in

triplicate in three independent experiments. Thus, the data at each Mn^{2+} concentration were based on 18 data points. Certain mutants with lower levels of transport had linear uptake for longer time periods so kinetic measurements in these cases included data at 3 minutes in addition to the 30 second and 60 second data points. Because the pH is constant, the transport velocity follows Michaelis-Menten kinetics with respect to $^{54}Mn^{2+}$ concentration (30). Initial estimates of K_m were made using a range of 0.2, 0.5, 1, 2.5 and 5.0 μM final concentration of Mn^{2+} and the concentrations of Mn^{2+} used were readjusted to be 3-fold above and below the estimated K_m value. Results were calculated by an analysis of a plot of v vs. [S] using the graphic analysis program Excel (Microsoft). Data from three independent runs (each done in triplicate) were averaged to give a value for apparent K_m and V_{max}, plus or minus the standard error of the mean.

Results

Identification of conserved residues in TMS-6

Our proposed secondary structural model for *E. coli* MntH is shown in Figure 1 (1) This model agrees with the proposed topology from another study (11). Conserved residues of TMS-6 were determined as previously described for the conserved acidic residues of the Nramp family (1). The most highly conserved residues in TMS-6 were Gly-205, Ala-206, Met-209, Pro-210, His-211, Leu-215, His-216, and Ser-217. These residues are indicated by a darkened circle in Figure 1. Based on a BLAST search, all of these residues, except for Leu-219, were 100% conserved among the top 100 homologs in the nonredundant database. (One homolog had Leu-219 changed to a methionine.) Such a high level of conservation is consistent with an important role of these residues with regard to structure and/or function.

Mutagenesis of conserved histidine residues

Because MntH is an H^+/Mn^{2+} symporter, it is reasonable to postulate that the two highly conserved histidine residues might play a role in the binding of Mn^{2+} and/or H^+. To investigate this possibility, the conserved histidine residues (His-211 and His-216) were first changed to nonionizable residues of similar size (i.e., histidine to glutamine). The histidines were also changed to a residue with a smaller side chain (alanine) and a larger ionizable residue (arginine). In some metal binding proteins, cysteine residues have been shown to substitute in metal binding for histidines (31-34), so the histidine residues were also changed to cysteine. The codon changes are described in Table 1. As seen in this table, the mutants were expressed at moderate to normal levels relative to wild-type.

Paired histidine residues have been reported to coordinate metals (24-26). To determine if metal transport could occur in the absence of these two highly conserved histidine residues, double mutations were also created. Each histidine was mutated to the same residue (e.g., H211Q/H216Q) by completing a second round of mutagenesis using a His-211 mutant as the template (see Table 1). Each double mutant was expressed at moderate to normal levels.

Transport characterization of wild-type, His-211, and His-216 mutant strains

The mutant strains were initially tested for $^{54}Mn^{2+}$ uptake at 0.3 μM, which is the K_m value for the wild-type strain (1). Figure 2 shows the transport levels of the mutants involving the conserved histidine residues (positions 211 and 216). The H211Q strain transported Mn^{2+} to levels near 90% of the wild-type strain whereas the H216Q strain transported to levels roughly two-thirds of the wild-type strain. In addition, a few other mutants transported Mn^{2+} at detectable rates, but less than 25% of wild-type. These included H211A, H216A, H211C, and H216C. The remaining mutants (H211R and H216R) showed transport rates that were indistinguishable from the background levels of transport seen in the knockout strain.

Because alteration of just one of the two histidine residues still showed significant Mn^{2+} transport, it was of interest to assess the effect of a double histidine mutation in TMS-6. Therefore, both His-211 and His-216 were mutated to the same residue (e.g., H211Q/H216Q) and each of the four double mutants were tested for Mn^{2+} uptake. Three of the double mutants showed transport of Mn^{2+} indistinguishable from the background, but the H211Q/H216Q double mutant still transported Mn^{2+} at very low levels but reliably above the background (Figure 3).

To further investigate the importance of the histidine residues in TMS-6, the mutants with measurable levels of transport were examined with regard to the kinetics of $^{54}Mn^{2+}$ uptake. These results are presented in Table 2. The H211Q strain had a moderately high V_{max} value and a K_m value that was not significantly different from the wild-type strain. Thus, it appears that His-211 is not critical for cation binding or transport. By comparison, the other mutants tested showed V_{max} values that were less than 25% of the wild-type strain. All mutant strains tested (H211A, H211C, H216A), except H216C, had K_m values similar to wild-type. The H216C strain had a slightly elevated K_m of 0.7 μM. It is possible that having a cysteine side chain in this position affected the overall tertiary structure of MntH, lowering the affinity for Mn^{2+} in the metal binding site. Additional supporting evidence for a disruption in overall structure by the cysteine substitution rather than direct interference with the metal binding site is shown by H216A having a K_m similar to wild-type.

A study from the Gros laboratory indicated that the two conserved histidines (His-267 and His-272) in mammalian Nramp2 play a role in the pH regulation of metal-transport function. It was found that alanine and cysteine substitutions, which had low activity at pH 6.0, were substantially rescued my lowering the pH (20). To determine if the homologous conserved histidine residues in the MntH protein from *E. coli* also played such a role, we examined the transport of two single mutants, H211Q and H216Q, and the corresponding double mutant at pH 5.0, 5.5, 6.0, and 6.5 (Figures 4 and 5). With regard to position 211, there was an increase in transport function from pH 6.5 to 5.0. However, the degree of change was not as dramatic as that seen in the mammalian protein in which transport function was very low at pH 6.0 and 6.5 (see ref. 20). For position 216, transport function changed in the opposite direction with the highest activity, relative to the wild-type strain, observed at pH 6.5.

Mutagenesis of other conserved residues along TMS-6

Certain residues surrounding the histidine pair (Gly-205, Ala-206, Met-209, Pro-210, Leu-215, and Ser-217) are also highly conserved throughout the Nramp family. To investigate their role in structure/function, each was changed to a variety of other residues, some substitutions preserving size of the side chain (i.e., Leu to Ile) and other substitutions changing the side chain size or chemistry (i.e., Met to Lys or Ser to Tyr). All mutations made to these sites are listed in Table 1. All mutations were expressed at moderate to normal levels compared to wild-type expression.

Transport characterization of mutants surrounding the histidine pair

The mutants at positions 205, 206, 209, 210, 215, and 217 were tested for Mn^{2+} transport at 0.3 μM Mn^{2+} (see Figures 6 and 7). Mutation of Gly-205 to Ala showed low levels of transport, whereas a mutation to Pro was completely defective. It should be noted that for all mutants not showing transport activity during the initial testing, further transport experiments were extended to 10 minutes to confirm the lack of Mn^{2+} transport activity. Preserving a smaller side chain volume as in the case of the A206G mutation caused a 50% decrease in transport activity, while substitution of a larger residue, leucine, abolished transport activity. Neither substitution of Ile or Lys for Met-209 showed transport activity, despite the similar side chain volumes of Met and Ile. Interestingly, mutation of Pro-210 to Gln or Ala decreased transport

activity to 25% of wild-type activity but mutation to a Gly abolished transport. Glycine has a smaller side chain volume than proline, but in our previous mutagenesis of Pro-37, substitution of a glycine was the only mutation where transport activity was still observed (1).

Histidine-216 is flanked by two highly conserved residues, Leu-215 and Ser-217. A number of mutations were made to each of these residues and the results are shown in Figure 7. Only the substitution of Ile to Leu still showed transport, albeit at low levels at 10 minutes, whereas changing the Leu to Ala or Val abolished transport. Of the four substitutions made to Ser-217, only S217T and S217A had measurable levels of transport. Transport was abolished in the S217Q and S217Y mutants. Serine, threonine, and tyrosine all have similar side chain chemistry with a hydroxyl group, but serine and threonine are more similar in side chain volume suggesting that preserving side chain volume is important to function at this position. Alanine is also fairly similar in side chain volume to serine whereas glutamine is much larger.

Kinetic analyses were performed on selected mutants (Table 3). G205A had a much lower V_{max} compared to wild-type MntH and a slightly elevated K_m of 0.7 μM. An indirect effect on metal binding is a probable cause of the elevated K_m considering the periplasmic end of TMS-6 may be positioned relatively close to the proposed binding site in the periplasmic ends of TMS-1-3. Mutation of glycine, a fairly small residue, to a slightly larger alanine may perturb the tertiary structure required for metal ion binding. Mutation of Gly-205 to an even larger residue, Pro, completely abolished transport. Kinetic measurements of P210A and P210Q were almost identical to each other, having a K_m similar to wild-type and a V_{max} of approximately 20% of wild-type MntH. L215I, S217A, and S217T strains also all had K_m values similar to wild-type and V_{max} values much lower than wild type: 1.3 nmol/mg/min, 4.3 nmol/mg/min. and 4.3 nmol/mg/min, respectively.

Discussion

In the current study, we investigated the role of two conserved histidine residues, His-211 and His-216, in *E. coli* MntH. In other proteins, histidine residues have been shown to play critical roles in transporter function. In transport proteins that transport or sense hydrogen ions, histidines may be directly involved in H^+ recognition (35,36). Histidine residues have also been implicated in pH-dependent regulation or modulation of a number of transport and channel proteins. For example, a single histidine residue determines the pH sensitivity of the cardiac and neuronal channel, HCN2 (37). Also, a single histidine is important for the pH regulation of the cardiac gap-junction protein connexin (38). In addition, histidines within proteins are capable of forming intra- and inter-molecular hydrogen bonds.

Other roles for histidine residues include substrate recognition and the interaction of helices during conformational changes. In the EAAC1 transporter (a glutamate/H^+ symporter), a single histidine residue (His-295) was hypothesized to be the proton acceptor because mutation of this residue to Arg, Thr, and Asn led to a non-functional protein (39). However, a more recent study examined the effects of additional substitutions to His-295 by changing this residue to Cys and Gln and revisiting the H295N mutation. H295N and H295C can still bind glutamate and H^+ even though the protein has little to no transport activity (40). Interestingly, substitution to glutamine maintained transport levels indistinguishable from wild-type. This suggested that His-295 is not protonated at physiological pH and does not contribute to proton transport. It appears that the side chain volume and/or length of His-295 is important for preserving overall protein structure or conformational changes that occur during transport. In addition, Gln can substitute for the NH (ε) of the histidine ring, acting as a hydrogen bond donor (41). His-295 may act as a hydrogen donor to an unidentified acceptor, and this interaction may be critical for function. This would explain the ability of Gln to substitute for His without affecting protein function.

The conserved histidine residues mutated in our study have also been investigated in the mouse Nramp2 homolog. The Gros laboratory examined the effects of mutating the histidine pair in TMS-6 (20). His-267 (equivalent to *E.coli* His-211) and His-272 (*E.coli* His-216) were each changed to alanine, cysteine, and arginine, and double mutants were also created. They found all mutants except H267C/H272C to be stably expressed in the membrane when expressed in a yeast double mutant (smf1/smf2) strain and when transfected into CHO cells. Each mutation was tested for Fe^{2+} and Co^{2+} (pH 6.0) transport in CHO cells. H267A, H267R, H272R, H267A/H272A, and H267R/H272R were all inactive for transport in both cases. Only H267A and H272C had significant transport activity compared to wild-type Nramp2. Upon lowering the pH of the assay to 5.0, wild-type Nramp2 maintained the same level of transport activity for Fe^{2+} and Co^{2+}, but H267A, H267C, and H272C showed increased transport at the lower pH, whereas H272A, H267A/H272A, which had been inactive at pH 6.0, were rescued at lower pH levels. They also made the observation that His-267 was more sensitive to mutation than His-272. The authors suggested that the histidine pair may be involved in the pH regulation of transport. In another study, Mackenzie et al. monitored metal-ion uptake, currents, and intracellular pH in wild-type and histidine mutants of rat Nramp2 expressed in *Xenopus* oocytes (42). They concluded that His-272 (equivalent to His-216 in *E. coli* MntH) is critical for coupling of metal ion transport to H^+ transport. Mutation of His-272 to alanine or arginine disrupted the coupling observed in wild-type Nramp2.

With regard to MntH in *E. coli*, Chaloupka et al. mutated both of the histidine residues (His-211 and His-216) in *E.coli* MntH (21). Several different single mutations were made: H211Y, H211A, H216A, and H216R, but no double mutants were created. The tyrosine mutation was chosen based upon the results of their evolutionary analysis of the Nramp family. Tyrosine is the most prevalent substitution for His-211 in the phylogenetic outgroup. In terms of size and hydrophobicity, it is a conservative substitution, but tyrosine exposes an acidic proton instead of the basic amino group of histidine. Sensitivity to metals was reduced in H211Y, and no transport was detected with Mn^{2+} although co-transport of Cd^{2+} and H^+ was detected at low levels. H211A preserved metal sensitivity (but not as sensitive as wild-type) and demonstrated transport of H^+ and Cd^{2+}, Fe^{2+}, and Mn^{2+} at pH 4.7. The authors concluded that His-211 is structurally and functionally important. However, it was not found to be essential because some activity was maintained with both mutations to His-211. Mutation of His-216 to Ala preserved transport activity of metal ions and H^+, but changing this residue to Arg abolished transport activity. H211A was observed to be less sensitive to mutation than H216A, which is the opposite of what was observed with mouse Nramp2 (20). In a more recent study, a H211Y mutant in MntH was shown to have an elevated K_m value and negligible transport at pH 7.5, indicating that position 211 may be important for both metal binding and pH dependence (23).

However, our results indicate that His-211 and His-216 do not play a critical role in metal binding. Substitutions at these sites had K_m values that were similar to the wild-type strain (see Table 2). Also, our results do not suggest a major role of His-211 or His-216 with regard to pH regulation of metal transport. At position 211, the H211Q mutant showed a modest increase in transport function from pH 6.5 to 5.0. However, the degree of change was not as dramatic as that seen in the mammalian protein in which transport function of certain mutants was very low at pH 6.0 and 6.5 (see ref. 20). For the H216Q mutant, transport function changed in the opposite direction with the highest activity, relative to the wild-type strain, observed at pH 6.5. Taken together, our results do not strongly support a role of the conserved histidine residues with regard to pH regulation of the transporter. Instead, the effects of side-chain volume changes are consistent with a role in conformational changes associated with transport. The glutamine substitutions had the highest levels of transport, and this residue is the closest in side chain volume to histidine. Arginine is a larger side-chain compared to histidine, and the increase

in size in these positions (211 and 216) abolished Mn^{2+} transport. Likewise, cysteine and alanine are smaller, and replacing His-211 or His-216 with this residue decreased transport.

Similarly, the other conserved residues (G205, A206, M209, P210, L215, and S217) seem to be important for transport function, but do not seem to be directly involved in metal binding. In all cases, mutations at these sites had apparent K_m values that were similar to the wild-type strain, but V_{max} values that were substantially reduced. Those substitutions with side-chain volumes most similar to the wild-type residue tended to have the highest activities.

Translocation of substrates by secondary active transporters requires conformational changes that promote conversion between an outwardly accessible and an inwardly accessible substrate binding site (43,44). Crystal structures of other secondary active transporters show that the helices surround a central cavity perpendicular to the plane of the membrane and a pseudo-twofold symmetry is observed in the folding of the helices into their tertiary structure (45-48). In the case of the glycerol-3-phosphate transporter from *E.coli*, each half of the protein forms two 3-helix bundles (46). This arrangement has been observed with other membrane transport proteins. A "rocker-switch" type of motion of transmembrane helices during substrate transport has been proposed based upon modeling with the crystal structure for the glycerol-3-phosphate transporter and other transporters with solved crystal structures (46-48). At the interface between the two "halves" of the protein, the periplasmic ends of the helices would separate as their cytoplasmic ends come together. Movements of the helices and their side chains are necessary for this "rocker-switch" motion to occur.

The conserved residues identified in this study could potentially lie on a face or faces of TMS-6 in MntH and be indispensable for function without playing a specific role in Mn^{2+} or H^+ binding. This idea could be further tested by directly measuring the binding of Mn^{2+} to the wild-type or mutant proteins. If mutations in TMS-6 that inhibit transport do not have a direct effect on metal binding, such an observation would be consistent with their role in conformational changes.

Critically important faces of transmembrane helices have been identified in the lactose permease prior to the availability of a crystal structure. Site-directed muutagenesis studies of loop 2/3 and TMS-2 of lactose permease suggested that the topology of TMS-2 is important for function and stability of the lactose permease (49-52). A similar observation was made with regard to Loop 8/9 and TMS-8 of the lactose permease suggesting structural symmetry between the two halves of the protein before the symmetry was comfirmed by crystallography studies (53-57). In TMS-8 of lactose permease, mutations along one face have detrimental effects on the initial rate of lactose transport and the maximal velocity of transport without significantly affecting the apparent K_m values for lactose binding when the mutation alters the side chain volume of the residues (53). Likewise, in the current study, the effects of mutating conserved residues along TMS-6 could be interpreted as having a negative impact on a conformationally sensitive interface in MntH.

Acknowledgments

This work was supported by a seed grant from the Biotechnology Institute of the University of Minnesota. Heather Haemig has been supported by the NIH Biotechnology Training Grant (IT32-GM08347).

References

1. Haemig HA, Brooker RJ. Importance of conserved acidic residues in mntH, the Nramp homolog of *Escherichia coli*. J Membr Biol 2004;201(2):97–107. [PubMed: 15630547]
2. Vidal SM, Malo D, Vogan K, Skamene E, Gros P. Natural resistance to infection with intracellular parasites: isolation of a candidate for Bcg. Cell 1993;73(3):469–485. [PubMed: 8490962]

3. Gunshin H, Mackenzie B, Berger UV, Gunshin Y, Romero MF, Boron WF, Nussberger S, Gollan JL, Hediger MA. Cloning and characterization of a mammalian proton-coupled metal-ion transporter. Nature 1997;388(6641):482–488. [PubMed: 9242408]
4. Mulero V, Searle S, Blackwell JM, Brock JH. Solute carrier 11a1 (Slc11a1; formerly Nramp1) regulates metabolism and release of iron acquired by phagocytic, but not transferrin-receptor-mediated, iron uptake. Biochem J 2002;363(Pt 1):89–94. [PubMed: 11903051]
5. Forbes JR, Gros P. Divalent-metal transport by NRAMP proteins at the interface of host-pathogen interactions. Trends Microbiol 2001;9(8):397–403. [PubMed: 11514223]
6. Papp-Wallace KM, Maguire ME. Manganese trnasport and the role of manganese in virulence. Annu Rev Microbiol 2006;60:187–209. [PubMed: 16704341]
7. Anderson ES, et al. The Manganese Transporter MntH Is a Critical Virulence Determinantfor *Brucella abortus* 2308 in Experimentally Infected Mice. Infection and Immunity 2009;77:3466–3474. [PubMed: 19487482]
8. Cellier M, Prive G, Belouchi A, Kwan T, Rodrigues V, Chia W, Gros P. Nramp defines a family of membrane proteins. Proc Natl Acad Sci U S A 1995;92(22):10089–10093. [PubMed: 7479731]
9. Makui H, Roig E, Cole ST, Helmann JD, Gros P, Cellier MF. Identification of the *Escherichia coli* K-12 Nramp orthologue (MntH) as a selective divalent metal ion transporter. Mol Microbiol 2000;35 (5):1065–1078. [PubMed: 10712688]
10. Kehres DG, Zaharik ML, Finlay BB, Maguire ME. The NRAMP proteins of *Salmonella typhimurium* and *Escherichia coli* are selective manganese transporters involved in the response to reactive oxygen. Mol Microbiol 2000;36(5):1085–1100. [PubMed: 10844693]
11. Courville P, Chaloupka R, Cellier MF. Recent progress in structure-function analyses of Nramp proton-dependent metal-ion transporters. Biochem Cell Biol 2006;84(6):960–978. [PubMed: 17215883]
12. Silver S, Johnseine P, King K. Manganese active transport in *Escherichia coli*. Journal of Bacteriology 1970;104(3):1299–1306. [PubMed: 16559107]
13. Courville P, Chaloupka R, Veyrier F, Cellier MF. Determination of transmembrane topology of the *Escherichia coli* natural resistance-associated macrophage protein (Nramp) ortholog. J Biol Chem 2004;279(5):3318–3326. [PubMed: 14607838]
14. Fleming MD, Trenor CC 3rd, Su MA, Foernzler D, Beier DR, Dietrich WF, Andrews NC. Microcytic anaemia mice have a mutation in Nramp2, a candidate iron transporter gene. Nat Genet 1997;16(4): 383–386. [PubMed: 9241278]
15. Fleming MD, Romano MA, Su MA, Garrick LM, Garrick MD, Andrews NC. Nramp2 is mutated in the anemic Belgrade (b) rat: evidence of a role for Nramp2 in endosomal iron transport. Proc Natl Acad Sci U S A 1998;95(3):1148–1153. [PubMed: 9448300]
16. Su MA, Trenor CC, Fleming JC, Fleming MD, Andrews NC. The G185R mutation disrupts function of the iron transporter Nramp2. Blood 1998;92(6):2157–2163. [PubMed: 9731075]
17. Blackwell JM, Searle S, Mohamed H, White JK. Divalent cation transport and susceptibility to infectious and autoimmune disease: continuation of the Ity/Lsh/Bcg/Nramp1/Slc11a1 gene story. Immunol Lett 2003;85(2):197–203. [PubMed: 12527228]
18. Patruta SI, Horl WH. Iron and infection. Kidney Int Suppl 1999;69:S125–S130. [PubMed: 10084296]
19. Ratledge C, Dover LG. Iron metabolism in pathogenic bacteria. Annu Rev Microbiol 2000;54:881–941. [PubMed: 11018148]
20. Lam-Yuk-Tseung S, Govoni G, Forbes J, Gros P. Iron transport by Nramp2/DMT1: pH regulation of transport by 2 histidines in transmembrane domain 6. Blood 2003;101(9):3699–3707. [PubMed: 12522007]
21. Chaloupka R, Courville P, Veyrier F, Knudsen B, Tompkins TA, Cellier MF. Identification of functional amino acids in the Nramp family by a combination of evolutionary analysis and biophysical studies of metal and proton cotransport in vivo. Biochemistry 2005;44(2):726–733. [PubMed: 15641799]
22. Cohen A, Nevo Y, Nelson N. The first external loop of the metal ion transporter DCT1 is involved in metal ion binding and specificity. Proc Natl Acad Sci U S A 2003;100(19):10694–10699. [PubMed: 12954986]

23. Courville P, Urbankova E, Rensing C, Chaloupka R, Quick M, Cellier MF. Solute carrier 11 cation symport requires distinct residues in transmembrane helices 1 and 6. J Biol Chem 2008;283(15): 9651–9658. [PubMed: 18227061]
24. Eicken C, Pennella MA, Chen X, Koshlap KM, VanZile ML, Sacchettini JC, Giedroc DP. A metal-ligand-mediated intersubunit allosteric switch in related SmtB/ArsR zinc sensor proteins. J Mol Biol 2003;333(4):683–695. [PubMed: 14568530]
25. Voss J, Hubbell WL, Kaback HR. Distance determination in proteins using designed metal ion binding sites and site-directed spin labeling: application to the lactose permease of *Escherichia coli*. Proc Natl Acad Sci U S A 1995;92(26):12300–12303. [PubMed: 8618889]
26. Eng BH, Guerinot ML, Eide D, Saier MH Jr. Sequence analyses and phylogenetic characterization of the ZIP family of metal ion transport proteins. J Membr Biol 1998;166(1):1–7. [PubMed: 9784581]
27. Kraft R, Tardiff J, Krauter KS, Leinwand LA. Using mini-prep plasmid DNA for sequencing double stranded templates with Sequenase. Biotechniques 1998;6(6):544–547. [PubMed: 3273187]
28. Martinez E, Bartolome B, de la Cruz F. pACYC184-derived cloning vectors containing the multiple cloning site and *lacZ* alpha reporter gene of pUC8/9 and pUC18/19 plasmids. Gene 1988;68(1):159–162. [PubMed: 2851489]
29. Sambrook, J.; Fritsch, EF.; Maniatas, T. Molecular Cloning: A Laboratory Manual. Cold Spring Harbor, NY: Cold Spring Harbor Laboratory; 1989.
30. Segel, I. Enzyme Kinetics. New York: Wiley and Interscience; 1975.
31. Nakagama H, Heinrich G, Pelletier J, Housman DE. Sequence and structural requirements for high-affinity DNA binding by the WT1 gene product. Mol Cell Biol 1995;15(3):1489–1498. [PubMed: 7862142]
32. Omichinski JG, Trainor C, Evans T, Gronenborn AM, Clore GM, Felsenfeld G. A small single-“finger” peptide from the erythroid transcription factor GATA-1 binds specifically to DNA as a zinc or iron complex. Proc Natl Acad Sci U S A 1993;90(5):1676–1680. [PubMed: 8446581]
33. Ghazaleh FA, Omburo GA, Colman RW. Evidence for the presence of essential histidine and cysteine residues in platelet cGMP-inhibited phosphodiesterase. Biochem J 1996;317(Pt 2):495–501. [PubMed: 8713077]
34. Worthington MT, Amann BT, Nathans D, Berg JM. Metal binding properties and secondary structure of the zinc-binding domain of Nup475. Proc Natl Acad Sci U S A 1996;93(24):13754–13759. [PubMed: 8943007]
35. Chen XZ, Steel A, Hediger MA. Functional roles of histidine and tyrosine residues in the H(+)-peptide transporter PepT1. Biochem Biophys Res Commun 2000;272(3):726–730. [PubMed: 10860823]
36. Wiebe CA, Dibattista ER, Fliegel L. Functional role of polar amino acid residues in Na^+/H^+ exchangers. Biochem J 2001;357(Pt 1):1–10. [PubMed: 11415429]
37. Zong X, Stieber J, Ludwig A, Hofmann F, Biel M. A single histidine residue determines the pH sensitivity of the pacemaker channel HCN2. J Biol Chem 2001;276(9):6313–6319. [PubMed: 11096117]
38. Ek JF, Delmar M, Perzova R, Taffet SM. Role of histidine 95 on pH gating of the cardiac gap junction protein connexin43. Circ Res 1994;74(6):1058–1064. [PubMed: 8187275]
39. Zhang Y, Pines G, Kanner BI. Histidine 326 is critical for the function of GLT-1, a ($Na^+ + K^+$)-coupled glutamate transporter from rat brain. J Biol Chem 1994;269(30):19573–19577. [PubMed: 7913472]
40. Tao Z, Grewer C. The conserved histidine 295 does not contribute to proton cotransport by the glutamate transporter EAAC1. Biochemistry 2005;44(9):3466–3476. [PubMed: 15736956]
41. Fersht, A. Structure and mechanism in protein science: a guide to enzyme catalysis and protein folding. Vol. xxi. New York: W.H. Freeman; 1999. p. 631
42. Mackenzie B, Ujwal ML, Chang MH, Romero MF, Hediger MA. Divalent metal-ion transporter DMT1 mediates both H(+) -coupled Fe(2+) transport and uncoupled fluxes. Pflugers Arch 2006;451 (4):544–558. [PubMed: 16091957]
43. West IC. Ligand conduction and the gated-pore mechanism of transmembrane transport. Biochim Biophys Acta 1997;1331(3):213–234. [PubMed: 9512653]
44. Tanford C. Translocation pathway in the catalysis of active transport. Proc Natl Acad Sci U S A 1983;80(12):3701–3705. [PubMed: 6574508]

45. Hunte C, Screpanti E, Venturi M, Rimon A, Padan E, Michel H. Structure of a Na+/H+ antiporter and insights into mechanism of action and regulation by pH. Nature 2005;435(7046):1197–1202. [PubMed: 15988517]

46. Huang Y, Lemieux MJ, Song J, Auer M, Wang DN. Structure and mechanism of the glycerol-3-phosphate transporter from *Escherichia coli*. Science 2003;301(5633):616–620. [PubMed: 12893936]

47. Faham S, Watanabe A, Besserer GM, Cascio D, Specht A, Hirayama BA, Wright E, Abramson J. The Crystal Structure of a Sodium Galactose Transporter Reveals Mechanistic Insights into Na+/Sugar Symport. Science 2008;321:810–813. [PubMed: 18599740]

48. Abramson J, Smirnova I, Kasho V, Verner G, Kaback HR, Iwata S. Structure and mechanism of the lactose permease of *Escherichia coli*. Science 2003;301(5633):610–615. [PubMed: 12893935]

49. Jessen-Marshall AE, Paul NJ, Brooker RJ. The conserved motif, GXXX(D/E)(R/K)XG[X](R/K)(R/K), in hydrophilic loop 2/3 of the lactose permease. J Biol Chem 1995;270(27):16251–16257. [PubMed: 7608191]

50. Jessen-Marshall AE, Brooker RJ. Evidence that transmembrane segment 2 of the lactose permease is part of a conformationally sensitive interface between the two halves of the protein. J Biol Chem 1996;271(3):1400–1404. [PubMed: 8576130]

51. Jessen-Marshall AE, Parker NJ, Brooker RJ. Suppressor analysis of mutations in the loop 2-3 motif of lactose permease: evidence that glycine-64 is an important residue for conformational changes. J Bacteriol 1997;179(8):2616–2622. [PubMed: 9098060]

52. Green AL, Anderson EJ, Brooker RJ. A revised model for the structure and function of the lactose permease. Evidence that a face on transmembrane segment 2 is important for conformational changes. J Biol Chem 2000;275(30):23240–23246. [PubMed: 10807929]

53. Green AL, Brooker RJ. A face on transmembrane segment 8 of the lactose permease is important for transport activity. Biochemistry 2001;40(40):12220–12229. [PubMed: 11580298]

54. Green AL, Hrodey HA, Brooker RJ. Evidence for structural symmetry and functional asymmetry in the lactose permease of Escherichia coli. Biochemistry 2003;42(38):11226–11233. [PubMed: 14503872]

55. Pazdernik NJ, Jessen-Marshall AE, Brooker RJ. Role of conserved residues in hydrophilic loop 8-9 of the lactose permease. J Bacteriol 1997;179(3):735–741. [PubMed: 9006028]

56. Pazdernik NJ, Cain SM, Brooker RJ. An analysis of suppressor mutations suggests that the two halves of the lactose permease function in a symmetrical manner. J Biol Chem 1997;272(42):26110–26116. [PubMed: 9334175]

57. Pazdernik NJ, Matzke EA, Jessen-Marshall AE, Brooker RJ. Roles of charged residues in the conserved motif, G-X-X-X-D/E-R/K-X-G-[X]-R/K-R/K, of the lactose permease of *Escherichia coli*. J Membr Biol 2000;174(1):31–40. [PubMed: 10741430]

Abbreviations

Nramp	natural resistance-associated membrane protein
TMS	transmembrane segment
MES	2-N-morpholino ethane sulfonic acid
TES	N-Tris [hydroxymethyl] methyl-2-aminoethanesulfonic acid)
TPCK	Tosyl phenylalanyl chloromethyl ketone
PMSF	phenylmethylsulfonyl fluoride

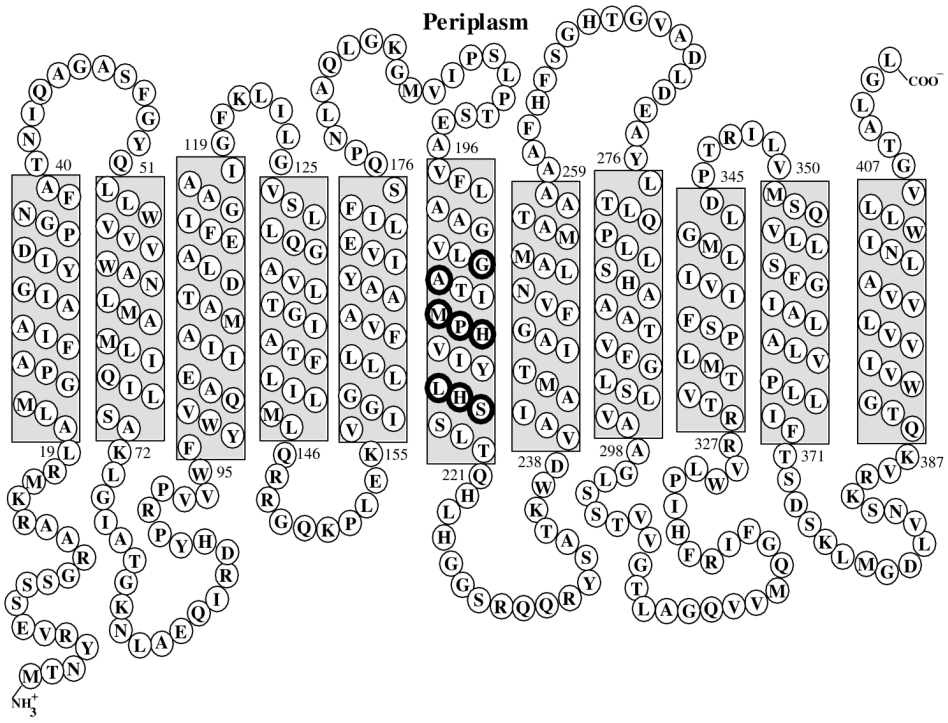

Figure 1. Secondary structure topology model of the *E. coli* Nramp homolog, MntH

Conserved residues mutated in this study are shown with a darkened circle. The model was generated as previously described (1).

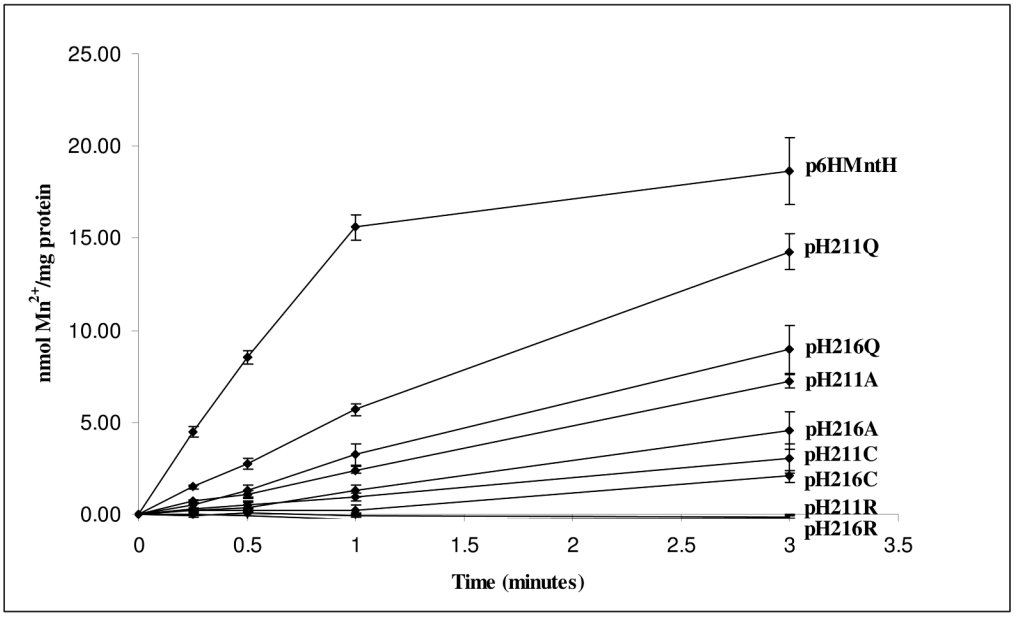

Figure 2. Transport characterization of wild-type and histidine mutants

The transport of $^{54}Mn^{2+}$ was measured at an external concentration of 0.3 μM at 37°C as described under Materials and Methods.

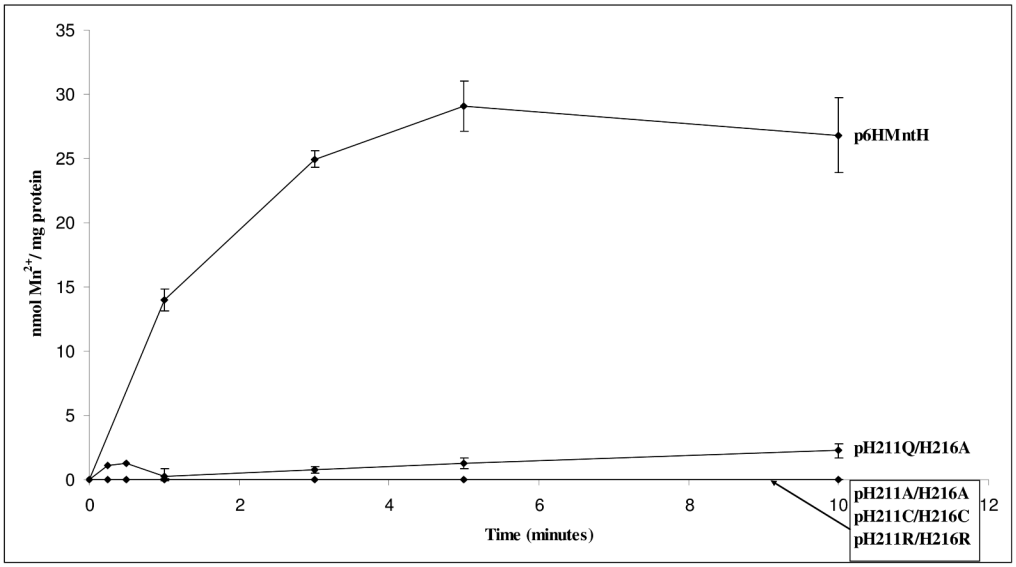

Figure 3. Transport characterization of wild-type and double histidine MntH mutants

The transport of $^{54}Mn^{2+}$ was measured at an external concentration of 0.3 μM at 37°C as described under Materials and Methods.

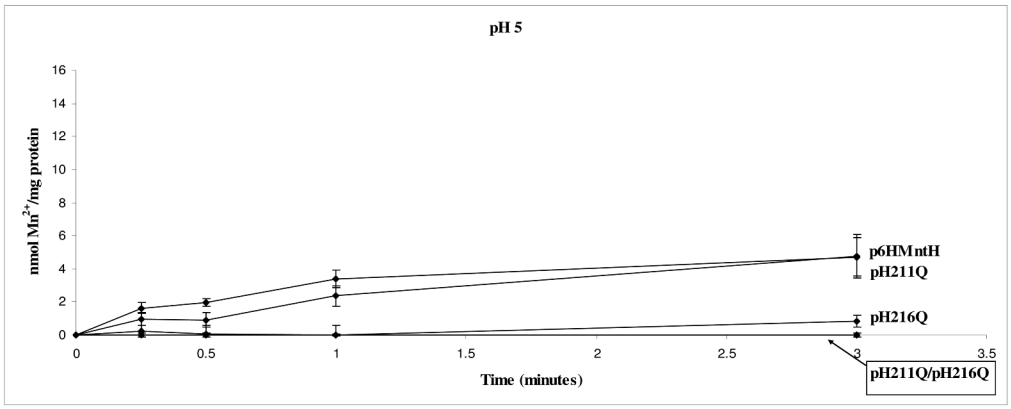

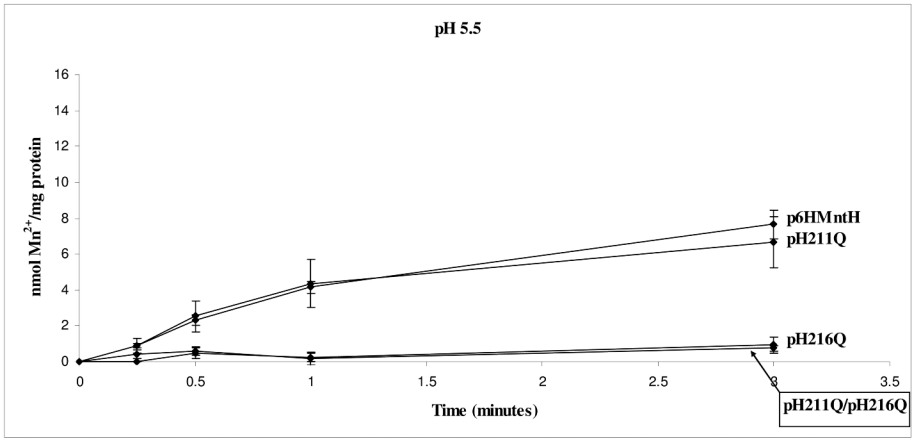

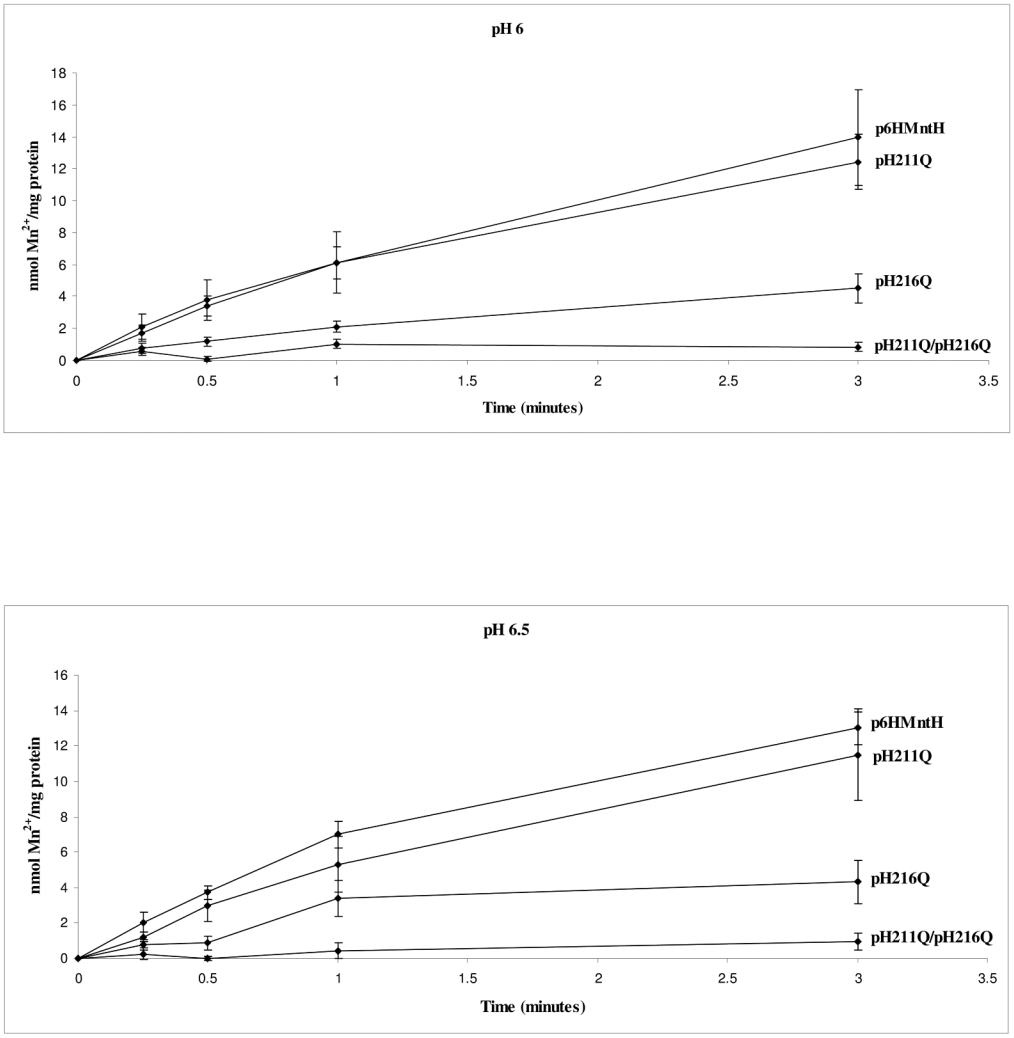

Figure 4. Transport characterization of wild-type, H211Q, and H216Q mutants at pH 5.0 to pH 6.5

The transport of $^{54}Mn^{2+}$ was measured at an external concentration of 0.3 μM at 37°C as described under Materials and Methods.

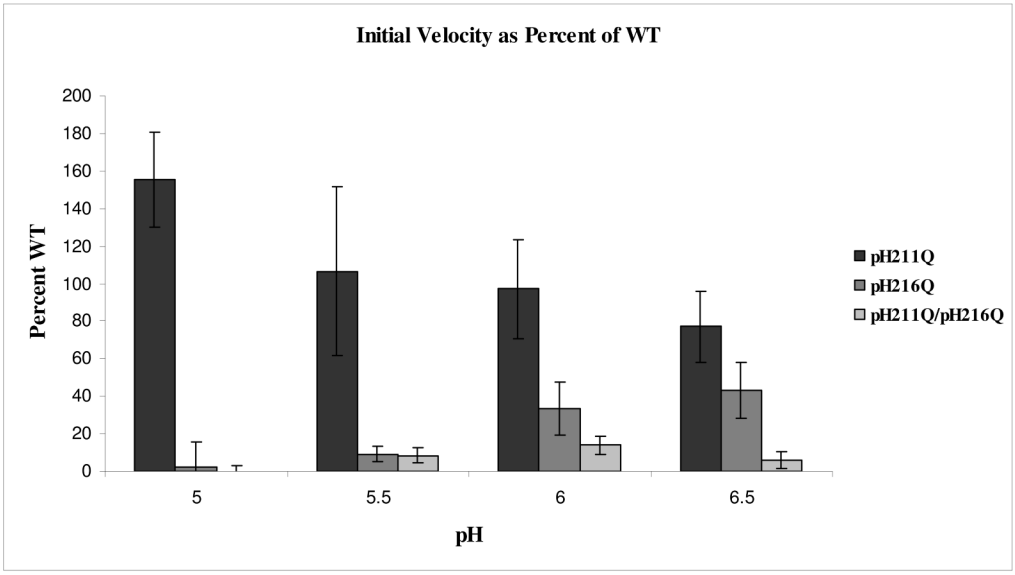

Figure 5. Relative transport rates of H211Q, H216Q, and H211Q/H216Q mutants at pH 5.0 to pH 6.5

The transport of $^{54}Mn^{2+}$ was measured at an external concentration of 0.3 μM at 37°C as described under Materials and Methods. Initial rates were determined and are expressed as a percentage of the wild-type rate at each pH.

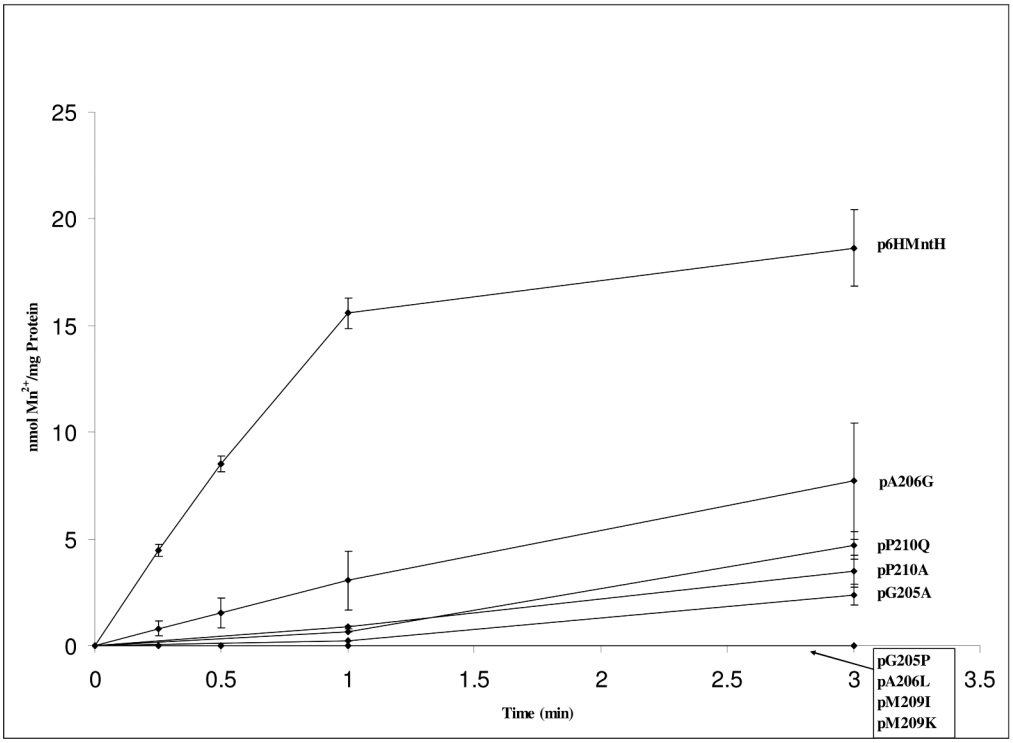

Figure 6. $^{54}Mn^{2+}$ uptake in wild-type and mutant strains that have alterations to conserved residues: Gly-205, Ala-206, Met-209, and Pro-210

The transport of $^{54}Mn^{2+}$ was measured at an external concentration of 0.3 μM at 37°C as described under Materials and Methods.

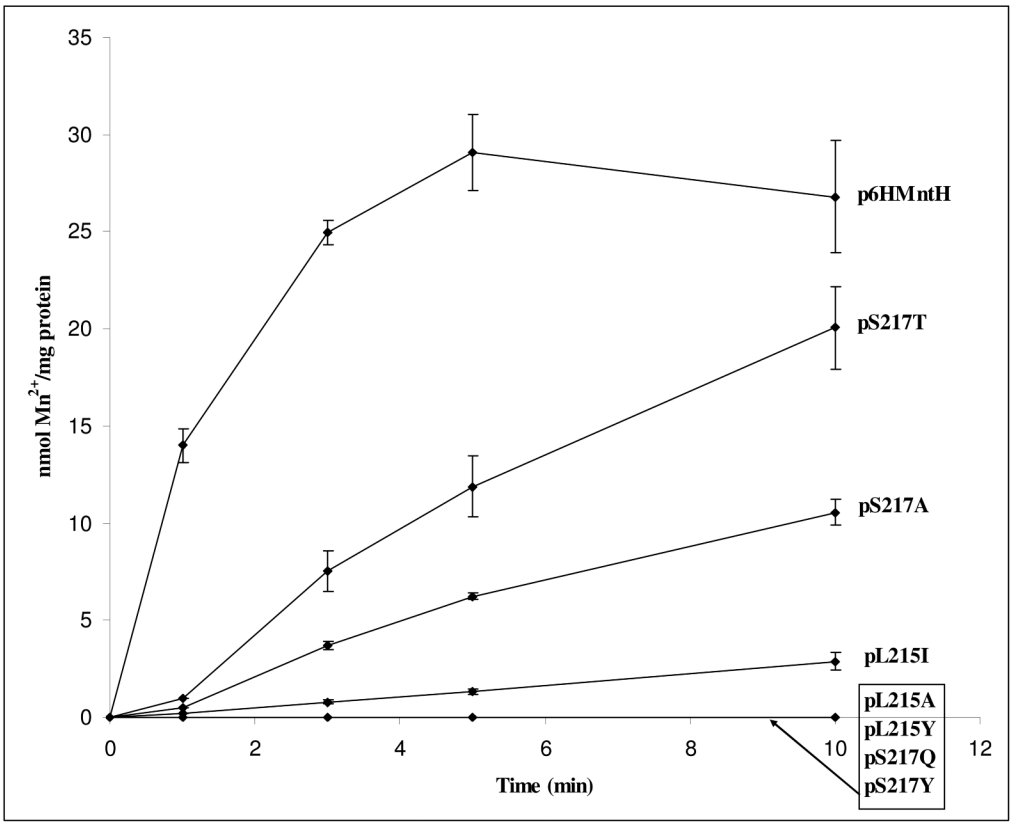

Figure 7. $^{54}Mn^{2+}$ uptake in 6-His-wild-type and mutant strains that have alterations to conserved residues: Leu-215 and Ser-217

The transport of $^{54}Mn^{2+}$ was measured at an external concentration of 0.3 μM at 37°C as described under Materials and Methods.

Table 1

Bacterial strains and plasmids

Strain	Relevant characteristics	Reference
MM2115	Strain MM1925 (*E. coli* K12 wild-type F^-/lambda$^-$/IN(*rrnD-rrnE*) with a kan^R insertion into the *mntH* gene	(10)

Plasmids	Description	Reference
pSU2718	Hybrid pACYC184/pUC18 cloning vector with a chloramphenicol resistance marker and *lac* promoter	(28)
p6HMntH	pSU2718, with the wild-type *mntH* gene under the control of the *lac* promoter plus a 6-Histidine tag is located at the amino terminus of MntH	(1)

Mutation[a]	Codon change	Protein Expression (% 6Hwild-type)[b]
G205A	GGG to GCC	102.0 ± 11
G205P	GGG to CCG	99.8 ± 2
A206G	GCG to GGC	87.3 ± 4
A206L	GCG to CTG	80.1 ± 5
M209I	ATG to ATC	87.2 ± 9
M209K	ATG to AAA	80.6 ± 12
P210A	CCG to GCC	81.8 ± 11
P210G	CCG to GGG	77.8 ± 6
P210Q	CCG to CAA	77.7 ± 5
H211A	CAT to GCT	61.0 ± 8
H211C	CAT to TGT	67.7 ± 12
H211Q	CAT to CAG	82.1 ± 7
H211R	CAT to CGC	80.0 ± 11
L215A	TTG to GCG	88.3 ± 7
L215I	TTG to ATC	74.0 ± 28
L215V	TTG to GTC	80.7 ± 12
H216A	CAC to GCC	86.3 ± 10
H216C	CAC to TGC	82.3 ± 9
H216Q	CAC to CAG	93.8 ± 9
H216R	CAC to CGG	81.8 ± 2
S217A	TCC to GCG	84.1 ± 6
S217Q	TCC to CAG	79.2 ± 1
S217T	TCC to ACG	77.2 ± 46
S217Y	TCC to TAT	75.4 ± 2
H211A/H216A	see single mutant	90.7 ± 10
H211C/H216C	see single mutant	85.8 ± 44
H211Q/H216Q	see single mutant	81.1 ± 36
H211R/H216R	see single mutant	78.5 ± 31

[a] The designated mutations were made using plasmid p6HMntH as the starting material.

[b] Expression levels were measured in strain MM2115 containing the plasmid with the wild-type *6HmntH* gene or a *6HmntH* gene with the designated mutation as described under Materials and Methods.

Table 2

Kinetic characterization of wild-type and substitutions of the conserved histidine residues

Strain	Apparent K_m[a] ± S.E.M. (μM)	Apparent V_{max}[a] ± S.E.M. (nmol·mg^{-1} ·min^{-1})
6HMntH (wild-type)	0.3 ± 0.1	19.2 ± 7.2
H211A	0.3 ± 0.1	4.1 ± 0.1
H211C	0.3 ± 0.1	2.6 ± 0.7
H211Q	0.2 ± 0.1	8.1 ± 0.8
H216A	0.2 ± 0.0	1.7 ± 0.2
H216C	0.7 ± 0.1	3.4 ± 0.0

[a]Kinetics measurements were made as described under Materials and Methods.

Table 3
Kinetic characterization of wild-type and substitutions of the other conserved residues

Strain	Apparent K_m[a] ± S.E.M. (μM)	Apparent V_{max}[a] ± S.E.M. (nmol·mg^{-1} ·min^{-1})
6HMntH (wild-type)	0.3 ± 0.1	19.2 ± 7.2
G205A	0.7 ± 0.2	3.6 ± 0.3
P210A	0.3 ± 0.1	2.6 ± 0.3
P210Q	0.3 ± 0.1	3.9 ± 0.9
L215I	0.2 ± 0.0	1.3 ± 0.3
S217A	0.3 ± 0.1	4.3 ± 1.4
S217T	0.1 ± 0.0	4.3 ± 0.1

[a] Kinetics measurements were made as described under Materials and Methods.